ACS APPLIED MATERIALS & INTERFACES

www.acsami.org

Research Article

Cellulose Nanofiber-Reinforced MXene Membranes as Stable Friction Layers and Effective Electrodes for High-Performance Triboelectric Nanogenerators

Chenyang Xing, Yun Tian, Zejue Yu, Zihao Li, Bo Meng,* and Zhengchun Peng*

Cite This: *ACS Appl. Mater. Interfaces* 2022, 14, 36741−36752

Read Online

ACCESS | Metrics & More | Article Recommendations | Supporting Information

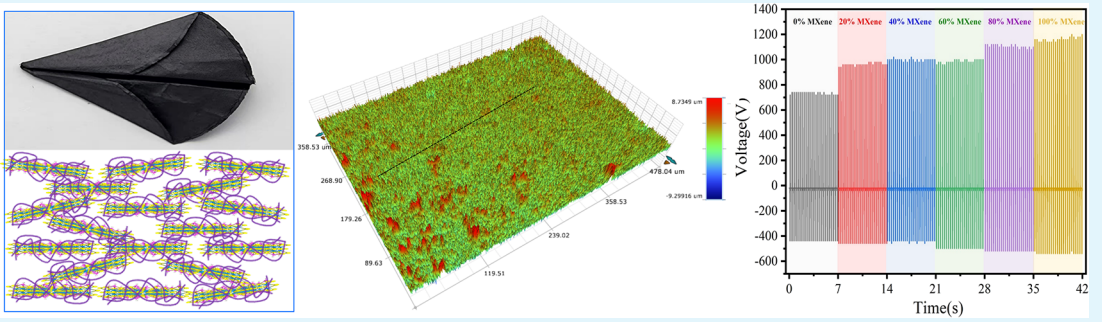

ABSTRACT: In this work, MXene films incorporating cellulose nanofibers (CNFs) with a spider-web-like structure were fabricated using a facile vacuum-assisted filtration method. The CNFs significantly improved the flexibility and stability of the MXene membranes. The resulting composites functioned well as electrodes and friction layers in triboelectric nanogenerators (TENGs) when paired with either polytetrafluoroethylene (PTFE) as an electropositive material or nylon as an electronegative material. A membrane containing 20 wt % CNFs in conjunction with PTFE was extremely effective during the prolonged operation of a TENGs, generating an output voltage in excess of 1120 V at a frequency of 3.5 Hz. The surface charge density of this device was as high as 100 μC m^{-2}. When paired with nylon, the MXene/CNF film produced a surface charge density of over 60 μC m^{-2}. The microstructures on the rough surface of these membranes, together with the presence of −F and other polar terminations on the MXene, are responsible for the high performance of the nanocomposite. This work demonstrates that MXenes are not necessarily equivalent to PTFE within the triboelectric series and suggests that the MXene-based friction layer could greatly enhance the performance of TENGs.

KEYWORDS: *triboelectric material, nanogenerator, MXene, cellulose nanofiber, nanocomposite*

1. INTRODUCTION

Two-dimensional (2D) carbides, nitrides, and carbonitrides, also known as MXenes, have recently attracted a great deal of interest in the fields of energy,[1] environmental,[2] and biomedical research.[3] The unique structures and intriguing physicochemical properties of MXenes are distinct from those of other 2D materials, such as graphene, black phosphorous,[4] tellurene,[5] and multiphase transition-metal dichalcogenides.[6] As an example, MXenes are highly conductive and are thus able to act as effective conductive fillers in polymer matrices and as solid or liquid electrodes in energy harvesting devices. MXenes also possess abundant surface functional groups, such as highly electronegative fluorine (F) atoms that originate from the use of HF during the preparation of these materials. The presence of polar hydroxy (−OH) groups and −O atoms on MXene nanosheets also allows these materials to exhibit adjustable hydrophilicity and polarity. It is also possible to employ 2D MXenes as building blocks to assemble three-dimensional (3D) films,[7−9] hydrogels,[10] aerogels,[11−14] and fibers,[15] either with or without other one-dimensional (1D) or 2D components. These 3D MXenes can display multiple functionalities, including high electrical conductivity, excellent thermal conductivity, compressibility, porosity, and even optoelectronic responses.

Triboelectric nanogenerators (TENGs) have emerged as a promising energy harvesting technology over the past decade,[16−19] as these devices can allow various sources of mechanical energy to be effectively converted into electricity.[20−22] This technology has numerous applications in self-

Received: June 14, 2022
Accepted: July 26, 2022
Published: August 4, 2022

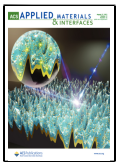

powered systems,[23−25] biomedical sensors,[26,27] and intelligent tactile units.[28−30] As a consequence of the many advantages of MXenes noted above, there has also been many efforts devoted to developing MXene-based TENGs.[31−33] The first attempt to fabricate TENGs from MXenes was reported by Yury's group in 2017.[34] This prior work showed that MXenes spray-coated onto glass substrates had triboelectric characteristics similar to those of polytetrafluoroethylene (PTFE) and so did not generate an output voltage when combined with electronegative PTFE in a single-electrode configuration. Yury suggested that these two materials may appear at the same location in the triboelectric series as a consequence of the surface −F atoms on both. MXenes were also found to function as an electronegative friction layer and as a conductive layer (i.e., an electrode). To date, MXenes have been primarily employed as conductive nanofillers to increase the conductivity or dielectric permittivity of polymers, and MXene-enhanced polymers have applications as high-performance friction layers. Examples include MXene/polymer electrospun nanofibers[35−39] and MXene/elastomer composites.[40,41] MXenes have also been utilized as electrodes in TENGs. As an example, Ma's group reported a stretchable TENG fabricated from 1D cellulose nanofibers (CNFs) integrated with an MXene dispersion as a liquid electrode in conjunction with standard silicon rubber as a triboelectrification layer.[42] However, to the best of our knowledge, there have been few studies of pure MXenes or MXene-rich composites that simultaneously act as effective electrodes and triboelectrification layers (having electronegative or even electropositive characteristics) for high-performance output.[43−45] Such investigations could be helpful by precisely locating MXenes in the triboelectric series.

The present work reports the flexible MXene films modified with spider-web-like CNFs to construct high-performance TENGs. These materials were prepared using a facile vacuum-assisted filtration (VAF) strategy and functioned as both highly conductive electrodes and robust friction layers with variable electronegativity in MXene-based TENGs. Results show that when paired with electronegative PTFE, MXene/CNF films containing 80 wt % MXenes were found to be electropositive and to generate output voltages of up to 1120 V at 3.5 Hz, with a charge density of approximately 100 μC m^{-2}. In contrast, when paired with electropositive nylon 6, these materials were determined to be electronegative and gave a voltage of over 650 V. The addition of CNFs was also shown to improve the mechanical properties of MXene films to ensure robust, long-lived, and stable friction materials.

2. EXPERIMENTAL SECTION

2.1. Fabrication of CNFs. The CNFs were fabricated using a modification of a previously developed method.[46] Briefly, clean and dried garlic husks (5 g) were cut into small pieces and then added to an aqueous NaOH solution (200 g, 2.0 wt %) at room temperature. This dispersion was subsequently subjected to a hydrothermal treatment at 140 °C for 5 h after which the solid product was captured by centrifugation and then washed with water until the wash water was neutral. The resulting solid was oxidized in a mixture of aqueous solutions of NaClO and H_2SO_4 (NaClO: 300 g, 1.5 wt %; H_2SO_4: 200 g, 2.0 wt %) with heating at 80 °C for 6 h. During this reaction, the dispersion changed to a light yellow-green color. The dispersion was cooled and then sonicated for 1 h at 10 °C using a power level of 750 W, after which high-speed mixing was applied at 7000 rpm for 1 h while cooling the sample with a flow of water. Subsequent to these procedures, inorganic ions and residual acid were removed via a 5 days dialysis process in deionized water. This series of treatments provided a colloidal dispersion of CNFs with a concentration of 2.0 mg/mL as determined by filtration and weighing.

2.2. Preparation of 2D MXene Nanosheets. The 2D MXene nanosheets were prepared in several stages. Initially, a quantity of MAX Ti_3AlC_2 (2 g) was slowly added to an aqueous solution of HCl (40 mL, 9 M) containing LiF (2 g) at room temperature with stirring at 400 rpm for 30 min. This mixture was then heated at 40 °C for 24 h, after which the etched MAX was recovered by centrifugation and washed with water until the pH of the wash water was approximately 6. The multilayered $Ti_3C_2T_x$ (M-$Ti_3C_2T_x$) obtained from the procedure described above was intercalated in ethanol for 30 min at a sonication power of 750 W, followed by centrifugation at 9800 rpm to collect the product. Residual ethanol was removed by a single wash with water (40 mL) followed by centrifugation at the same speed. A single wash was applied because repeated washing cycles tended to exfoliate the M-$Ti_3C_2T_x$ such that it became more difficult to separate from the water. The collected M-$Ti_3C_2T_x$ was mixed with deionized water (20 mL) and subsequently sonicated for 10 min. To obtain a larger yield, the tube was continuously agitated by hand during the sonication process. This dispersion was then centrifuged at 3500 rpm for 10 min to collect the d-MXene nanosheets. Repeating the above sonification−centrifugation process was found to provide higher yields. Based on filtration and weighing, the concentration of MXenes was determined to be 2.6 mg/mL.

2.3. Preparation of MXene/CNF Films. In a typical trial, an MXene/CNF composite film was prepared using a vacuum-assisted filtration method. Briefly, different volumes of a MXene dispersion and a CNF dispersion were combined and thoroughly mixed using an oscillator at room temperature. Following this, the mixture was filtered through a porous mixed cellulose ester membrane to produce a film that was then dried in a vacuum oven at 60 °C. The amounts of the two solutions were varied to give films with MXene/CNF mass ratios of 20:80, 40:60, 60:40, or 80:20. As control samples, both neat MXenes and neat CNF membranes were also fabricated by a similar method.

2.4. Characterization of MXene Films. The morphology of each 2D MXene film was investigated by transmission electron microscopy (FEI Tecnai G2 F30 and JEM-1230) and by field emission scanning electron microscopy (Hitachi, SU800). X-ray photoelectron spectroscopy was conducted using a PHI-5000 VersaProbe II (ULVAC-PHI) instrument with monochromatic Al Kα radiation. Raman measurements (machine model, Horiba LabRAM HR800) were performed at room temperature with an excitation wavelength of 532 nm. X-ray diffraction (XRD) patterns were obtained using a BrukerD8 instrument with a scanning speed of 1°/min. The Fourier transform infrared spectroscopy (FTIR, Bruker Tensor) instrument was applied to detect the physical interactions of samples. The mechanical properties of the MXene membranes were ascertained using an Instron instrument (model 5966) at a strain rate of 0.05 mm/s. At least three samples were tested and average values are reported. The electrical properties of specimens were determined using a four-point probe instrument. The surface roughness of samples was evaluated using a white light scanning interferometer (ContourGT-K, Bruker, Germany). The water contact angle (WCA) of each sample was determined using a DSA100 machine (Data-Physics, Germany) at ambient temperature. Five positions on each sample were measured, averaged, and reported as the contact angle.

2.5. Measurements of the Basic Performance of TENGs. A digital oscilloscope (ZLG, ZDS2024B Plus) was employed to measure the output voltages of TENG specimens via a 100 MΩ oscilloscope probe. The short-circuit current was determined using a low-noise current preamplifier (Stanford, SR570), while the transferred charge was measured by charging a 0.1 μF capacitor. Periodic mechanical stimuli applied to the TENGs were generated by a linear direct current motor (Tianli Motor Co., 5GU-15KB).

https://doi.org/10.1021/acsami.2c10551
ACS Appl. Mater. Interfaces 2022, 14, 36741−36752

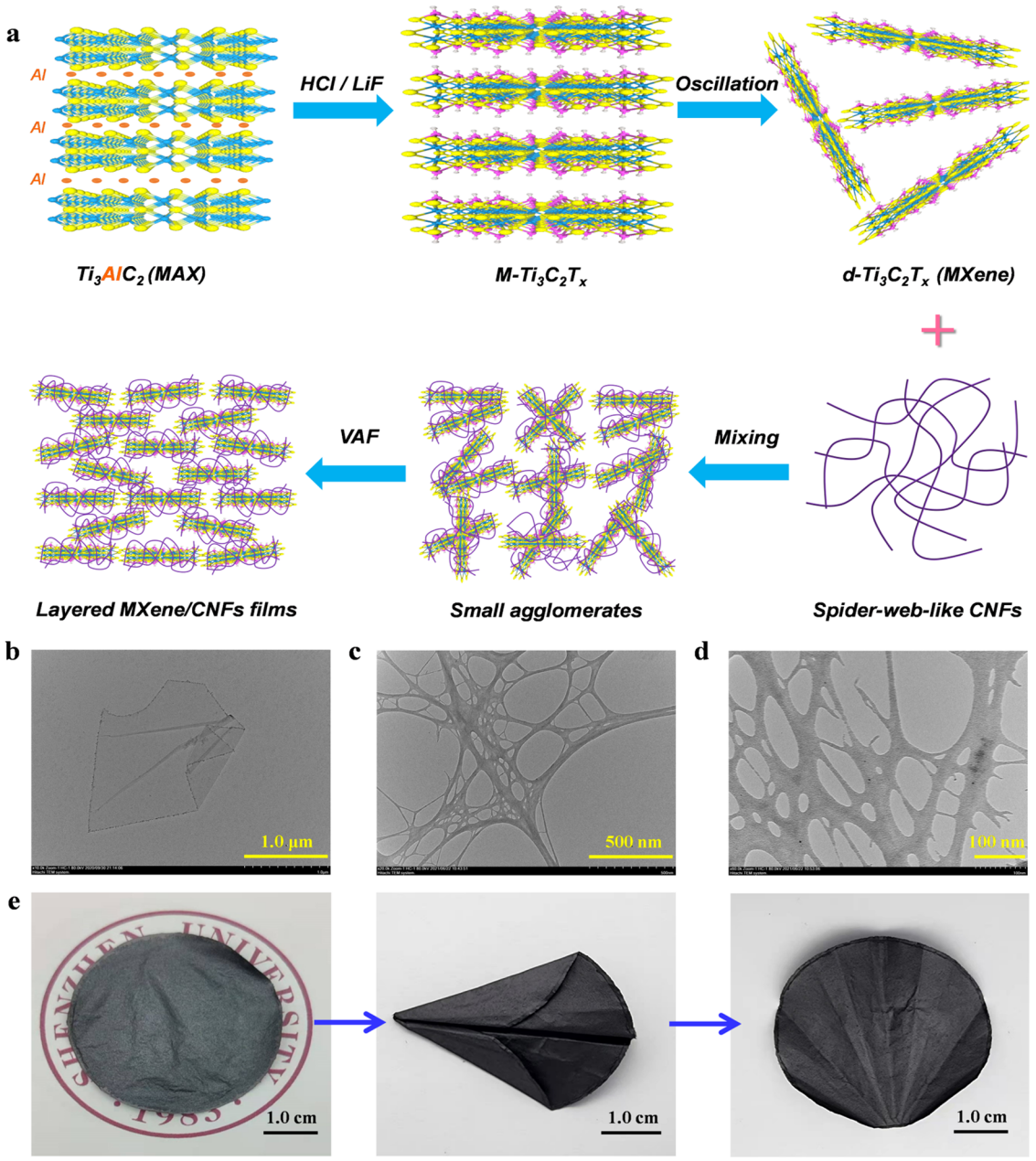

Figure 1. (a) Scheme illustrating the preparation of 2D MXene nanosheets, spider-web-like CNFs, and MXene/CNF composite films. (b) Transmission electron microscopy (TEM) image of an individual 2D MXene nanosheet. (c and d) TEM images of the CNFs. (e) Photographic images of an MXene/CNF film with 80 wt % MXene produced using VAF over top of the Shenzhen University logo and a film specimen before and after being folded into the shape of a paper plane.

3. RESULTS AND DISCUSSION

3.1. Synthesis and Characterization of MXene/CNF Membranes. In this study, 2D MXene nanosheets were prepared by a chemical exfoliation method, as illustrated in Figure 1a, and so were terminated by abundant polar surface groups, such as −F, −OH, and −O. These polar groups can cause the MXene surface to be positively or negatively charged, which is determined by references. These nanosheets had lateral dimensions of several micrometers (Figure 1b), and larger MXenes such as these tend to exhibit good film-forming properties. CNFs were fabricated using a multistep strategy and exhibited a unique spider-web-like morphology with a highly entangled structure containing many micro- or nano-scale holes, as shown in Figure 1c,d. These structures were very different from the typical individual 1D morphologies of CNFs.[46] Inorganic MXene nanosheets normally show metal-like conductivity but are physically weak when assembled into films. In contrast, organic CNFs are ductile and flexible but are electrically insulating. It was therefore expected that the integration of CNFs into MXene films might provide materials with improved mechanical properties while still maintaining excellent conductivity. A standard VAF method was used to construct MXene/CNF composite films, as illustrated in Figure 1a. The resulting membranes (Figure 1e) were sufficiently flexible such that they could be folded into the shape of a plane without cracking (Figure 1e) and could still preserve excellent electrical property even after several

https://doi.org/10.1021/acsami.2c10551
ACS Appl. Mater. Interfaces 2022, 14, 36741−36752

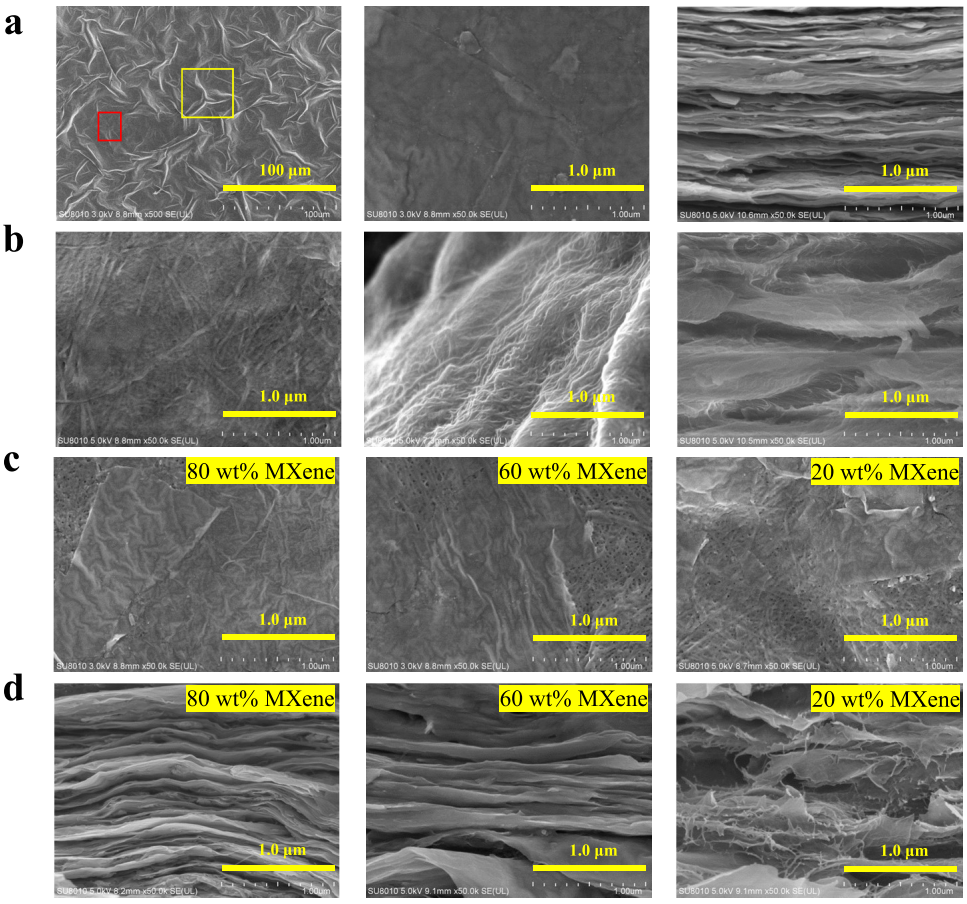

Figure 2. Morphological characterization of MXene/CNF composite films and their components. TEM images showing the surface and cross-section morphologies of a neat MXene film (a), a neat CNF film (b), and MXene/CNF films containing 80, 60, and 20 wt % MXenes (c and d).

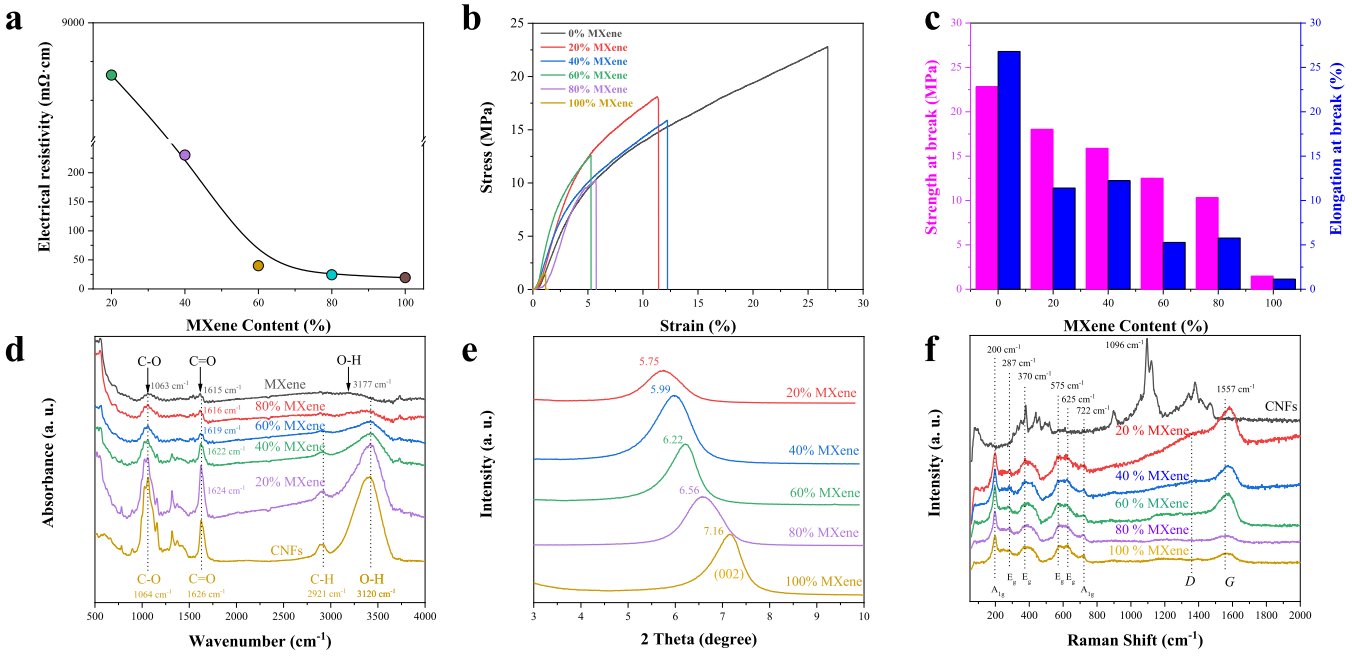

Figure 3. Structure and property characterization of MXene/CNF composite films and their components. (a) Electrical properties. (b, c) Mechanical properties. (d) FTIR spectrum. (e) XRD patterns. (f) Raman spectrum.

thousands of folding (Figure S1 in the Supporting Information).

The morphologies of the neat CNFs, neat MXenes, and the various composite films produced using different mass ratios are presented in Figure 2. Figure 2a (left) demonstrates that

https://doi.org/10.1021/acsami.2c10551
ACS Appl. Mater. Interfaces 2022, 14, 36741−36752

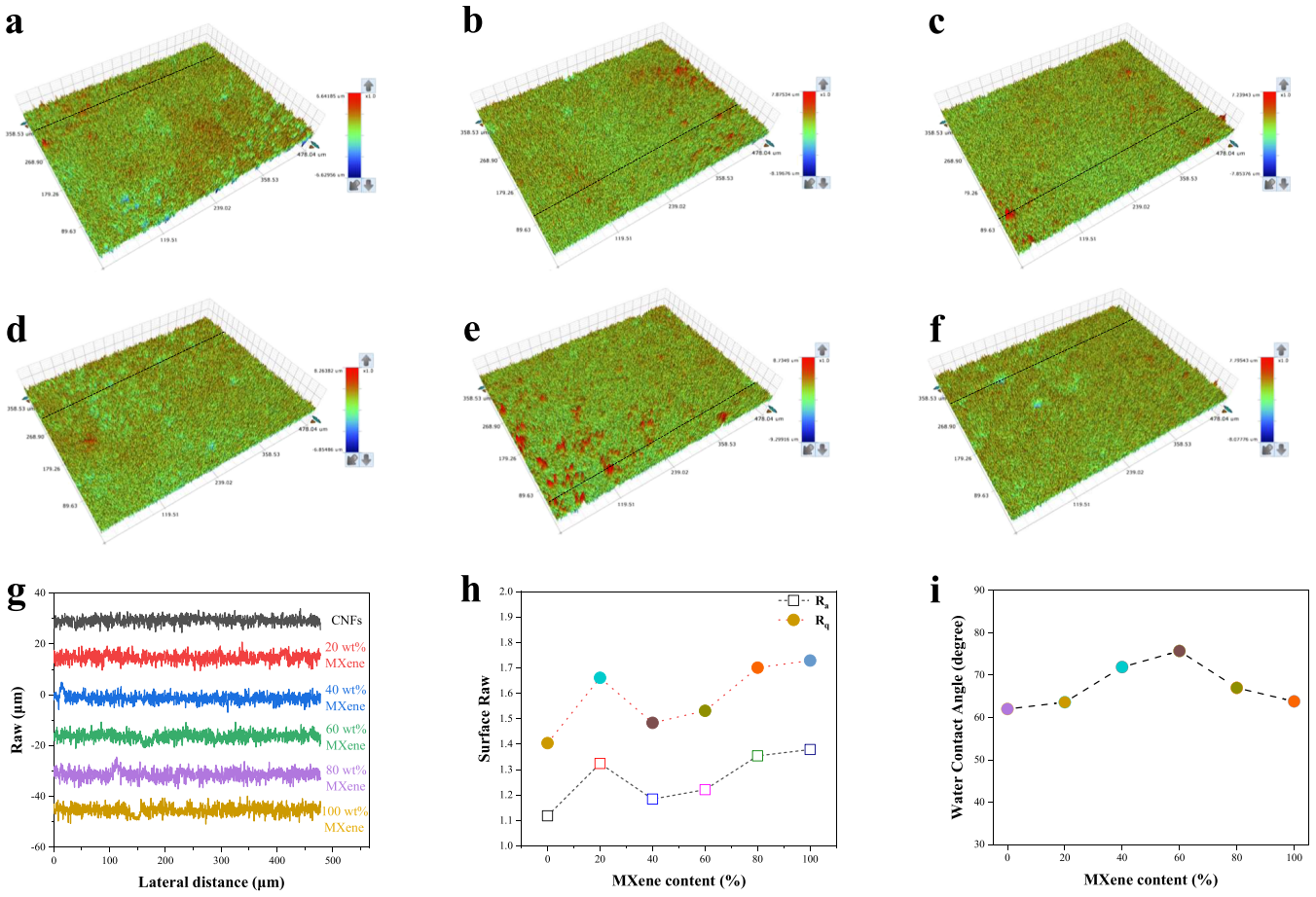

Figure 4. Surface topography and wetting behaviors of MXene films, CNF films, and their composite films. 3D height profiles of CNFs (a), MXene/CNF films with 20 wt % MXenes (b), 40 wt % MXenes (c), 60 wt % (d), 80 wt % (e), and MXene films (f). (g) Corresponding height profiles along the black line indicated. (h) Corresponding values of average roughness (R_a) and root mean square roughness (R_q) obtained from their 3D images. (i) Surface water contact angle (WCA) of various MXene/CNF films as a function of MXene content.

the neat MXene membrane had a wave-like undulating surface structure, as can be seen in the area within the yellow box. This result is attributed to the extrusion effect applied to the individual MXene nanosheets as they were stacked vertically during the filtration process and suggests a high degree of flexibility. This structure provided some degree of surface roughness, although the neat MXene film also contained a relatively flat region as indicated by the red box. The stacking of these MXene nanosheets can be observed in Figure 2a (middle), which presents a higher-magnification image. Typical layer-by-layer stacking in the neat MXene film is also apparent in the corresponding cross-sectional image in Figure 2a (right). In contrast, the neat CNF film exhibited an aggregated surface morphology (Figure 2b, left and middle) and a layer-like cross-section as a consequence of the spider-web-like structure (Figure 2b, right). Because of this structure, the filtration times of the neat CNF sample and of the MXene/CNF mixtures with low MXene contents (less than 10 wt %) were very short (less than 5 s for a 10 mL volume), indicating the potential for mass production. The MXene film containing 80 wt % MXenes was found to have a much rougher surface, as indicated by the clear wrinkles that can be observed on the individual MXene surfaces in Figure 2c. Similar structures were apparent on the specimens made with 60 and 20 wt % MXenes, as presented in Figure 2c. The MXene nanosheets were thin but wide, while the CNFs were relatively thick and porous (Figure 1c). During the VAF process, a vertical force was applied to the films that resulted in physical interactions between the components of the dispersion, so that they were stacked on one another in the vertical direction. This effect was responsible for the relatively rough surfaces of the MXene/CNF films. Figure 2d demonstrates that the distances between MXene nanosheets in the MXene/CNF films were also increased by the intercalation of the CNFs. In addition, the relatively irregular fracture morphology of the MXene/CNF film in Figure 2d suggests ductile rupture behavior based on strong physical interactions between the MXene nanosheets and CNFs.

The MXene/CNF ratio in the films had a pronounced effect on the electrical and mechanical properties of these materials. As shown in Figure 3a, the resistivity values of the films gradually decreased with increases in the MXene content, reaching a plateau at 60 wt % related to an electrical percolation threshold. Figure 3b,c demonstrates that the neat MXene film crumbled when drawn, with an extremely low elongation at break (1.2%) and a low tensile strength at break (1.5 MPa). The neat CNF film was both more flexible (26.8%) and stronger (22.8 MPa), and the addition of CNFs to the MXene films therefore improved the strain and tensile strength of these materials. Considering its slightly lower resistivity than those of MXene/CNF films (~40 mΩ·cm for 60 wt % MXenes and ~230 mΩ·cm for 40 wt % MXenes) and the obviously

https://doi.org/10.1021/acsami.2c10551
ACS Appl. Mater. Interfaces 2022, 14, 36741−36752

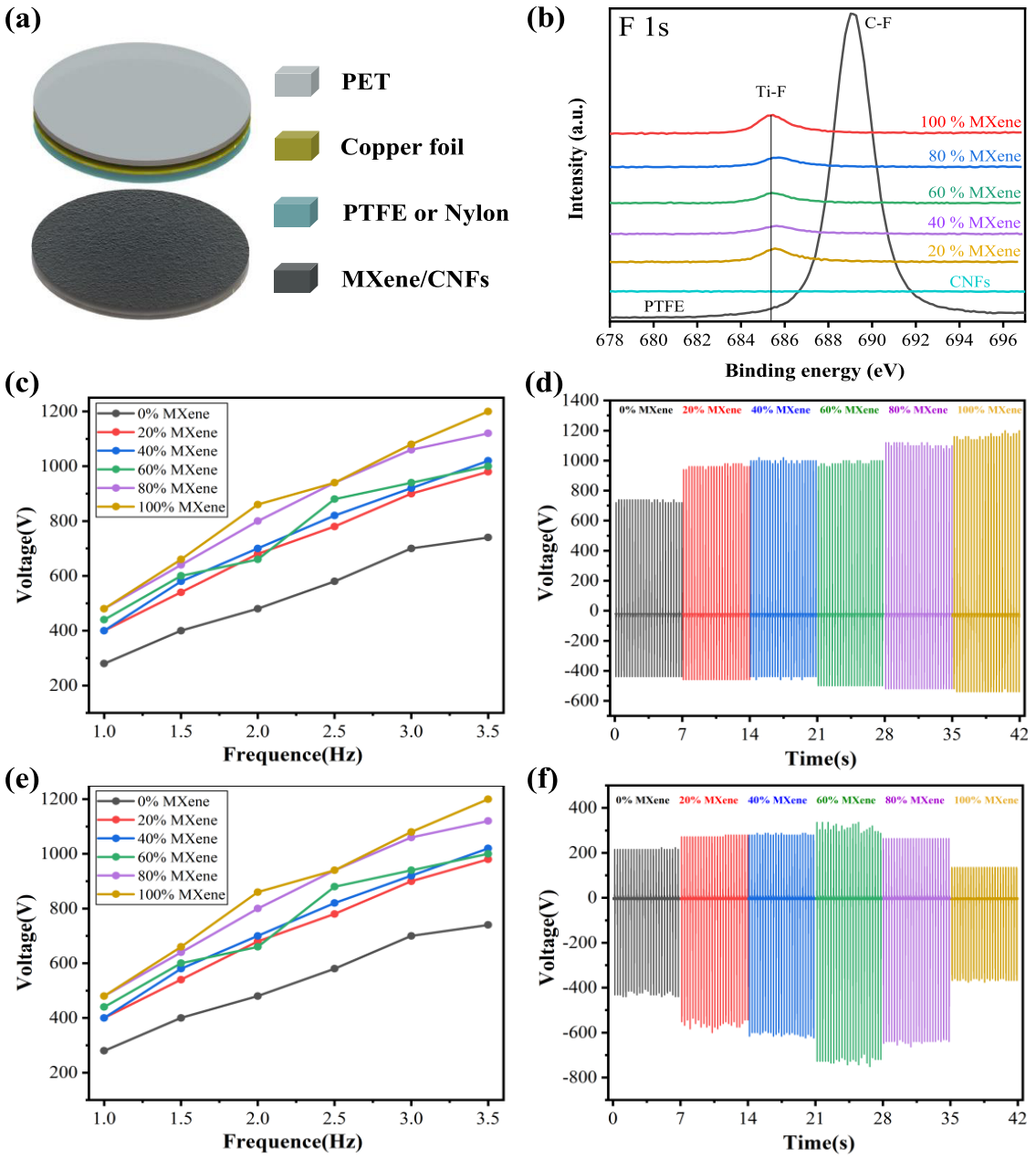

Figure 5. (a) Structure of the present MXene-based TENGs. (b) X-ray photoelectron spectra of specimens. Output voltages obtained from MXene/CNF−PTFE TENG devices (c) at various frequencies and (d) at a fixed frequency of 3.5 Hz. Output voltages obtained from MXene/CNF−nylon TENG devices (e) at various frequencies and (f) at a fixed frequency of 3.5 Hz.

increased ductility than that of the neat MXene film, an 80 wt % MXene sample (~24 mΩ·cm) was then selected for the fabrication of conductive layers and friction layers in the following TENG section. The physical interaction between MXenes and CNFs was evaluated using the FTIR spectrum in Figure 3d. MXenes have several surface functional groups, including −OH at 3177 cm^{-1}, carbonyl −C═O at 1615 cm^{-1}, and C−O at 1063 cm^{-1}. The −OH groups from MXenes show a broad absorption. In contrast, CNFs show strong and sharp absorption peaks of −OH and C═O groups at 3120 and 1626 cm^{-1}, respectively, together with the C−H and C−O strength vibrations at 2921 and 1064 cm^{-1}. In the cases of MXene/CNF films, with increasing MXene contents, the intensity of peaks assigned to −OH and C═O groups gradually decreased, companied by the broadening of half peak width (HPW) and the shift of wavelength to the middle between MXenes and CNFs. This observation suggests the possible interactions of −OH with C═O groups between MXenes and CNFs, i.e., hydrogen bonding interaction, which can well explain the improvement of mechanical properties of MXenes by adding CNFs (Figures 2d and 3b,3c). It should be noted that −F groups at the MXene surfaces may also contribute to the physical interactions between MXenes and CNFs by forming −F−H−O hydrogen bonds. The crystalline structures of the resultant MXene film, CNF film, and their composite films were evaluated by comparing their corresponding XRD patterns, as shown in Figures 3e and S2 in the supporting information. It is shown that the typical diffraction angle assigned to the (002) plane (Figure 3e) for MXenes decreased with the addition of CNFs in the MXene/CNF composite

https://doi.org/10.1021/acsami.2c10551
ACS Appl. Mater. Interfaces 2022, 14, 36741−36752

films. Besides, the (004) and (006) planes[47] (Figure S2) of MXenes also gradually become weak in the MXene/CNF composite films. This suggests an increased interlayer spacing of MXene sheets by integration of CNF components. Figure 3f shows the Raman spectrum of samples. The neat MXene film presents typical vibrational peaks at 200 and 722 cm^{-1}, assigned to the A_{1g} modes of $Ti_3C_2O_2$, and at 287 and 625 cm^{-1} attributed to the E_g modes of $Ti_3C_2(OH)_2$ and $Ti_3C_2F_2$,[48] respectively. The additional peaks at 370 and 575 cm^{-1} also correspond to the E_g vibration MXene. These peaks indicate the presence of the termination groups of −O, −OH, and −F on the MXene surface.[49] The clear G-band at 1557 cm^{-1} with a weak D-band can also be observed for MXene films. As for neat CNF films, a strong and sharp peak at 1096 cm^{-1} can be ascribed to the C−O ring and/or C−O−C glycosidic bond stretching of the CNFs.[50] In the cases of MXene/CNF films, the main vibration signals of MXenes can be observed, while the Raman signal from CNFs was indistinguishable. Besides, the G-band of MXenes, assigned to the graphite backbone (ordered sp^2 carbons), shows a blue shift with addition of CNFs, indicating an effective interaction between MXenes and CNFs.

Figure 4 illustrates the surface roughness of MXene/CNF films. A random surface area of 478 × 358 μm^2 was chosen in each sample. The typical 3D height profiles of each sample are shown in Figure 4a−f, which show that these VAF-induced films have a certain roughness, although they exhibit macroscopically smooth surfaces. By measuring the height vibration of the line indicated, the roughness of each sample can be qualitatively evaluated. As shown in Figure 4g, compared with the neat CNF film, neat MXene films present a slightly larger roughness, reflected by a higher span in height fluctuation. This is good in agreement with the wrinkled surface morphology of the neat MXene film. The largest roughness of MXene/CNF films was found in the case with 80 wt % MXene content, according to Figure 4e,g, with a clear height vibration. The calculated average roughness (R_a) and root mean square roughness (R_q) of MXene−CNF-based specimens are plotted in Figure 4h, as a function of MXene contents.

Both the two highest roughness parameters were found in the case of MXene/CNFs with 80 wt % content. The water contact angles (WCAs) of the samples in Figure 4i indicate that the MXene film, CNF film, and MXene/CNF composite films are all hydrophilic with WCA values not suppressing 90°, which may be a compromised result of their surface functional groups and surface roughness.

3.2. Characterization of TENGs. Yury's group first reported the concept of spin-coating MXenes to construct TENGs[34] and showed that a $Ti_3C_2T_x$-based MXene was both electronegative and very similar to PTTE in electronegativity. As a result, when acting as a friction layer, the MXene did not generate a voltage output in the PTFE. Zhai et al. used VAF-induced double component MXene films as the friction layer to pair with Nylon and the resultant TENGs show poor output performance. And their MXene films may exhibit insufficient mechanical properties to act as an electrode.[44] However, in the present study, MXene films made using VAF with or without CNFs were found to function both as effective electrodes and as stable friction layers in TENGs. The neat MXene film and the various MXene/CNF films were paired with PTFE or nylon 6 as electropositive and electronegative counterparts, respectively, to fabricate TENGs in contact-separation mode (Figure 5a). Characterization by X-ray photoelectron spectroscopy was used to evaluate the presence of F on the surfaces of the MXene-based films and the PTFE. As demonstrated in Figure 5b, the PTFE spectrum contained a more intense F peak at a higher binding energy compared with the peaks in the spectra of the MXene-based films. These results strongly suggest that the concentrations and polarities of the −F groups differed between the PTFE and the various MXene specimens, which was the basic concept used to construct the MXene-PTFE TENGs. Figure 5c summarizes the performances of TENGs based on neat MXene, neat CNF, and MXene/CNF films paired with PTFE. These data confirm that both the neat CNF and neat MXene membranes were able to serve as friction layers with PTFE to produce high voltages. As an example, the CNF−PTFE TENG generated a voltage of 700 V at a frequency of 3.5 Hz (Figure 5c). This result was not unexpected because the CNF membrane exhibited surface roughness and was electropositive in terms of the triboelectric series. However, it was surprising to find that the neat MXene-based membrane also functioned as a friction layer with PTFE and was able to generate a high output voltage of up to 1200 V (Figure 5c). Importantly, this voltage was considerably larger than that obtained using the neat CNF. It is also noted that MXenes are typically regarded as electronegative materials because of the abundant −F and −OH terminal groups on their surfaces and so would not be expected to generate a voltage when paired with a compact PTFE film.[34] In the case of the present work, two factors may explain this discrepancy. Compared with MXenes sprayed onto indium tin oxide glass in Yury's report,[34] the present MXene membranes manufactured using VAF likely had much rougher surfaces, as can be seen in Figure 2a. In addition, although the surfaces of the MXene made in this research had numerous −F and oxygen-containing groups, these materials were found to differ from PTFE in terms of polarity and electronegativity, as shown in Figure 5b. In fact, the neat MXene film made in this work was electropositive relative to PTFE.

Although it is of interest that the neat MXene film was able to function as an electropositive triboelectrification layer in a TENG, this material did exhibit peeling in response to friction, especially during prolonged usage. This effect was possibly a result of the rigidity of the inorganic MXene film. For this reason, the spider-web-like CNFs were integrated into the films to improve the stability of the MXene as a friction layer, with MXene/CNF mass-based ratios of 80:20, 60:40, 40:60, and 20:80. In the case of the 80:20 sample, a slightly decreased voltage of 1120 V was obtained at 3.5 Hz (Figure 5d) compared with that produced by the neat MXene membrane. Further increasing the CNF content in the membrane to 40, 60, and 80 wt % resulted in additional slight decreases in the output voltage, which remained above 950 V (Figure 5d). The addition of CNFs to the MXene also significantly improved the ductility of the material while greatly reducing the peeling effect. These results confirmed that incorporating CNFs enhanced the mechanical properties of the MXene membranes while maintaining their initial high output performance.

The performances of MXene/CNF−PTFE TENGs at 1.0, 1.5, 2.0, 2.5, and 3.0 Hz were also assessed, with the results provided in Figure 5c. The 80:20 specimen showed a gradual increase in voltage with increases in frequency and this trend was also exhibited by the other MXene/CNF samples. These data provided further evidence that the neat MXene and MXene/CNF membranes were able to work as effective

https://doi.org/10.1021/acsami.2c10551
ACS Appl. Mater. Interfaces 2022, 14, 36741−36752

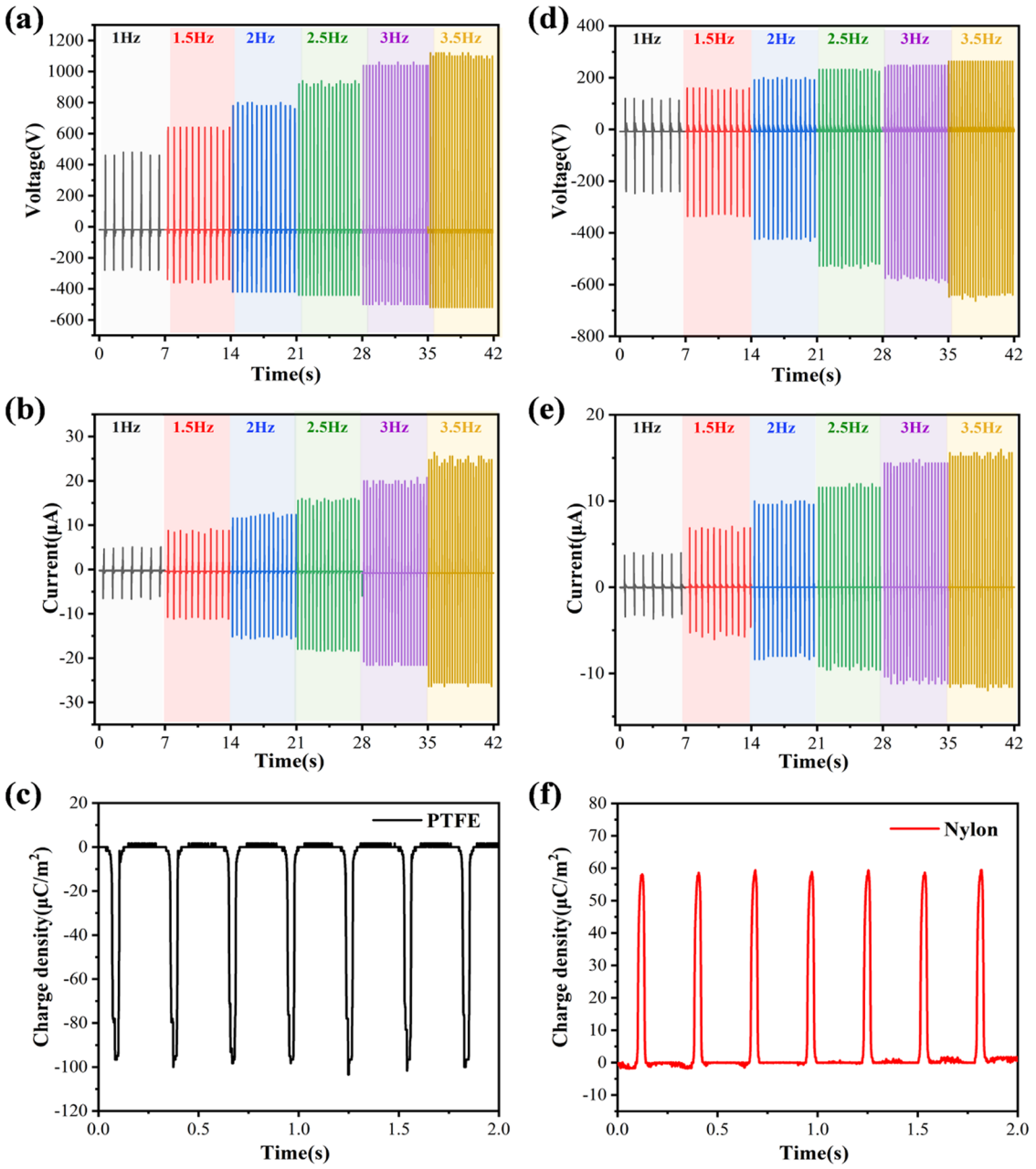

Figure 6. Output performances (including voltage, current, and surface charge density) of TENGs based on an MXene/CNF (80:20) film paired with (a, b, and c) PTFE or (d–f) nylon.

friction layers to generate high output voltages when combined with PTFE film. Based on the above results, it can be concluded that neat MXene and MXene/CNF films have potential as electropositive triboelectrification layers as well as electrodes in TENGs.

As shown in Figure 5e, both neat MXene and MXene/CNF membranes could also be used as electronegative materials to construct TENGs in conjunction with electropositive nylon material. In these trials, neat MXene and neat CNF films produced output voltages of 440 and 376 V at 3.5 Hz, respectively (Figure 5e), and this voltage was increased when using the MXene/CNF membranes. The highest voltage value was observed in trials with the sample having a 60% MXene content. It was also determined that this sample continued to exhibit the highest output voltage at all frequencies (Figure 5e,f). From these results, it is apparent that the neat MXene and MXene/CNF membranes produced using VAF were able to act as both electropositive and electronegative friction materials when paired with PTFE and nylon, respectively. As to the short-circuit currents, they showed similar trends to the output voltages. Figure S3 in the supporting information shows the short-circuit currents of the TENGs at a fixed frequency of 3.5 Hz.

The output performance of the MXene/CNF TENG containing the 80:20 membrane was assessed, with the results presented in Figure 6. When incorporating PTFE, this device showed increases in both the output voltage (Figure 6a) and current (Figure 6b) as the applied frequency was raised from 1 to 3.5 Hz. Similarly, when using nylon as the opposing friction layer, both the output voltage (Figure 6d) and current (Figure 6e) increased along with the frequency. However, the MXene/CNF (80:20) membrane was found to be much more effective

https://doi.org/10.1021/acsami.2c10551
ACS Appl. Mater. Interfaces 2022, 14, 36741−36752

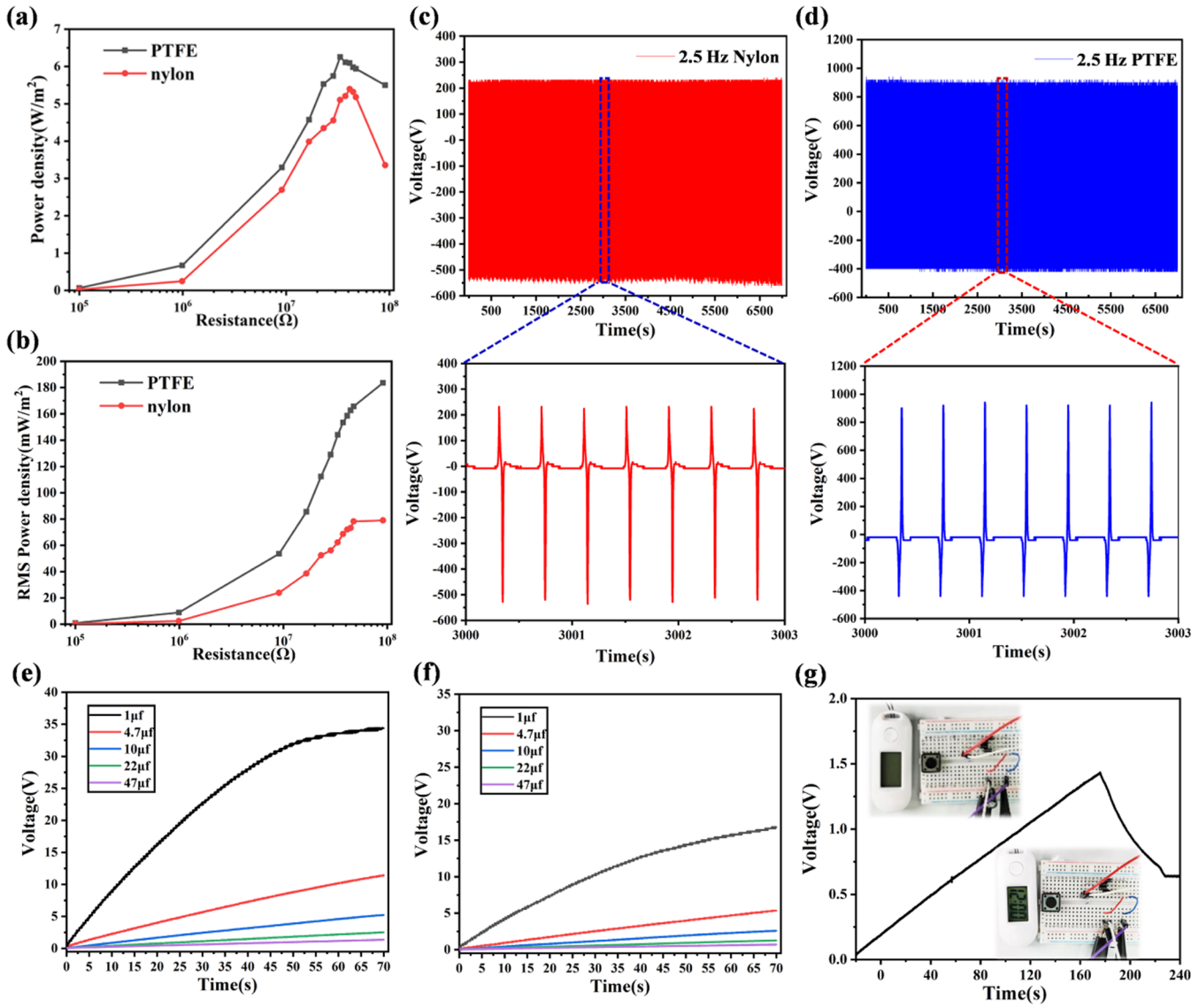

Figure 7. (a) Power density and (b) RMS power density data for TENGs based on MXene/CNF (80:20) films under different load resistors. The stability of the output voltage obtained from (c) MXene/CNF (80:20)−nylon TENG and (d) MXene/CNF (80:20)−PTFE TENG devices at a fixed frequency of 2.5 Hz. Charge performances of (e) MXene/CNF (80:20)−PTFE TENG and (f) MXene/CNF (80:20)−nylon TENG devices. (g) Data for charging of a commercial electronic watch using an MXene/CNF (80:20)−PTFE TENG.

when integrated with PTFE compared with nylon. When using PTFE, a maximum output voltage of 1120 V and a current of 25 μA were obtained at 3.5 Hz, which were far higher than the values of 650 V and 16 μA observed with nylon. Importantly, the MXene/CNF−PTFE TENG also exhibited a higher surface charge density ($\Delta\sigma_{sc}$) than that of an MXene/CNF−nylon TENG. As an example, a high $\Delta\sigma_{sc}$ value of 100 μC m^{-2} was obtained with the MXene/CNF−PTFE TENG (Figure 6c) relative to the value of 60 μC m^{-2} for the MXene/CNF−nylon TENG (Figure 6f). These data confirm the superiority of MXene/CNFs as electropositive friction layers in TENGs. The output performances of the TENGs using MXenes/CNFs (60:40) paired with PTFE and nylon were characterized as well. The results are illustrated in Figure S4 in the Supporting Information. 60 wt % MXene/CNF−PTFE TENG also shows higher outputs than 60 wt % MXene/CNF−nylon TENG. But the difference is smaller than the 80 wt % ones. The surface charge density of 60 wt % MXene/CNF−PTFE TENG is 86 μC m^{-2}. For 60 wt % MXene/CNF−nylon TENG, the value is 70 μC m^{-2}, which is in the middle of the 80 wt % MXene/CNF TENGs' surface charge density.

The power density and root mean square (RMS) power density of the TENG incorporating the MXene/CNF (80:20) film were also measured. Figure 7a shows that the PTFE-based TENG exhibited a gradual increase in power density as the external resistance was increased. The value reached a maximum of 6.25 W/m^2 at 33 MΩ followed by a decrease with further increase in the external resistance. A similar trend was also found in the case of the MXene/CNF−nylon TENG, but with a lower maximum power density of 5.39 W/m^2 at the same external resistance. Figure 7b indicates positive correlations of the calculated RMS power density values of the two TENGs with resistance. The maximum values were determined to be 183 mW m^{-2} for the PTFE-paired TENG and 78.9 mW m^{-2} at 90.9 MΩ for the nylon-paired TENG. As to the 60 wt % MXene/CNF TENGs, the RMS power density reached 144 mW m^{-2} when paired with PTFE and 110 mW m^{-2} when paired with nylon (Figure S5 in the supporting

https://doi.org/10.1021/acsami.2c10551
ACS Appl. Mater. Interfaces 2022, 14, 36741−36752

Table 1. Comparison of Device Conformation and Output Performance of Our MXene-/CNF-Based TENGs With the Similar Ones Recently Reported

MXene-based composites	form	counter layer	acted as friction layer	positive/ negative	acted as electrodes	voltage (V)	current density (μA cm^{-2})	power density (mW m^{-2})	surface charge density (μC m^{-2})	ref
MXene/CNFs	VAF films	PTFE	yes	positive	yes	~1120	~2.23	~6250	~100	this work
MXene/CNFs	VAF films	nylon	yes	negative	yes	~650	~1.43	~5390	~60	this work
porous PDMS/ MXene	spin-coating film	paper	yes	negative	no	~119	~2.75	~609	not given	40
PVA/MXene nanofiber film	electrospinning nanofiber mat	silk nanofiber film	yes	negative	no	~118.4	~1.8	~1087.6	not given	36
PVDF-TrFE/ MXene nanofibers	electrospinning nanofiber mat	nylon-11 nanofibrous	yes	negative	no	~270	~14	~4020	~533.33	38
PVDF/MXene nanofiber	electrospinning nanofiber mat	nylon 6/6	yes	negative	no	~724 V	~40.9	~11 200	~455	37
MXene/CNFs	aerogels	PVDF	yes	positive	no	~115.3	~0.25	~402.9	not given	45
alternated layered MXene films	VAF films	nylon	yes	negative	no	~34.63	~8.65	~100	~130	44
MXene/CNFs	spin-coating film	PTFE	yes	positive	yes	~24.9	~1.8	~1.2	~49	43
MXene	spraying-coating	PTFE	yes			0	0	0	0	34

information). The durability of each of the two MXene−CNF-based TENGs was also evaluated (Figure 7c,d). Both devices continued to generate stable output voltages even after 7000 cycles, indicating excellent durability and stability. The charge performance of the TENG made with the MXene/CNF (80:20) film was also ascertained. This device had a higher charging ability (Figure 7e) as indicated by a greater rate (higher slope) and increased charge capacitance compared with the MXene/CNF (80:20)−nylon TENG (Figure 7f). Furthermore, the MXene/CNF (80:20)−PTFE TENG was able to charge a 47 μF capacitor to approximately 1.5 V and so successfully power a commercial electronic watch (Figure 7g). Since the composite film exhibits good flexibility and conformability, we further performed an application using an 80 wt % MXene/CNF−PTFE TENG as a wearable active sensor for gesture recognition. As it is shown in Figure S6 in the Supporting Information, a 5 × 2 cm^2 sized TENG was attached to an adult's finger. The output voltage of the TENG varied when the knuckle bent at different angles. A gradual increase in the voltage can be observed as the angle was enlarged from 30 to 120°.

3.3. Comparison of Device Conformations and Output Performance. Table 1 shows the comparison of device conformation and output performance of our MXene/CNF−PTFE and MXene/CNF−nylon TENGs with other previously reported MXene or MXene−CNF-based TENGs. In terms of device structures, the VAF-induced-layered MXene/CNF films in this work can both act as positive or negative friction layers and effective electrodes, which distinguish from other MXene/polymer systems, including spin-coating films[40] and electrospun nanofibers[36−38] that were only used as friction layers. The alternated MXene films were previously used as friction layers but their mechanical properties were too weak to be used effectively as electrodes.[44] It is noted that similar MXene−CNF−aerogel−PVDF[45] and MXene−CNF-film−PTFE[43] had also been reported. However, the former was not conductive to be an electrode,[45] and the effective work of the latter lies on a PDMS substrate.[43] The above discussion indicates that our MXene/CNF TENGs not only have shown advantages of device conformation (effective electrodes, robust friction layers, and high flexibility) but also exhibited comparable as well as stable output performances,[43,44] which is very promising for practical energy harvesting.

4. CONCLUSIONS

MXene/CNF composite membranes, paired with either PTFE or nylon, were shown to function as high-performance friction materials in TENGs. The introduction of CNFs having a unique spider-web-like 1D morphology significantly improved the durability, stability, and even surface roughness of MXene films. The abundant wrinkles on the MXene surfaces originating from vacuum-assisted filtration, together with the various surface polar groups, allowed the MXene/CNF composites to act as either positive or negative friction layers in TENGs. The MXene/CNF (80:20)−PTFE−TENG system provided an output voltage of over 1120 V at a frequency of 3.5 Hz and a surface charge density of 100 μC m^{-2}, exceeding the values of 650 V and 60 μC m^{-2} for the MXene/CNF (80:20)−nylon−TENG counterpart. This result reveals the superiority of MXene/CNF films as the triboelectrically positive friction layer in TENGs. Similar conclusions were reached using specimens made in a variety of proportions of the MXene. The MXene/CNF-based TENGs also possessed excellent long-term stability for practical applications.

■ ASSOCIATED CONTENT

Supporting Information

The Supporting Information is available free of charge at https://pubs.acs.org/doi/10.1021/acsami.2c10551.

Resistance variation of the MXene/CNF (80:20) composite film before and after folding 1000, 2000, and 3000 times; XRD patterns of MXenes, CNFs, and their composite films; short-circuit currents of the TENG devices at a fixed frequency of 3.5 Hz; the output performances (including voltage, current, and surface charge density) of TENGs based on an MXene/CNF (60:40) film paired with PTFE or nylon; RMS power density of TENGs with the MXene/CNF (60:40) composite film under different load resistors; demon-

https://doi.org/10.1021/acsami.2c10551
ACS Appl. Mater. Interfaces 2022, 14, 36741−36752

stration of the application as a wearable active sensor for gesture recognition using an 80 wt % MXene/CNF–PTFE-based TENG (PDF)

AUTHOR INFORMATION

Corresponding Authors

Bo Meng − *Center for Stretchable Electronics and NanoSensors, Key Laboratory of Optoelectronic Devices and Systems of Ministry of Education, College of Physics and Optoelectronic Engineering, Shenzhen University, Shenzhen 518060, China*; Email: bomeng@szu.edu.cn

Zhengchun Peng − *Center for Stretchable Electronics and NanoSensors, Key Laboratory of Optoelectronic Devices and Systems of Ministry of Education, College of Physics and Optoelectronic Engineering, Shenzhen University, Shenzhen 518060, China*; orcid.org/0000-0002-7114-1797; Email: zcpeng@szu.edu.cn

Authors

Chenyang Xing − *Center for Stretchable Electronics and NanoSensors, Key Laboratory of Optoelectronic Devices and Systems of Ministry of Education, College of Physics and Optoelectronic Engineering, Shenzhen University, Shenzhen 518060, China*; orcid.org/0000-0002-2521-529X

Yun Tian − *Center for Stretchable Electronics and NanoSensors, Key Laboratory of Optoelectronic Devices and Systems of Ministry of Education, College of Physics and Optoelectronic Engineering, Shenzhen University, Shenzhen 518060, China*

Zejue Yu − *Center for Stretchable Electronics and NanoSensors, Key Laboratory of Optoelectronic Devices and Systems of Ministry of Education, College of Physics and Optoelectronic Engineering, Shenzhen University, Shenzhen 518060, China*

Zihao Li − *Center for Stretchable Electronics and NanoSensors, Key Laboratory of Optoelectronic Devices and Systems of Ministry of Education, College of Physics and Optoelectronic Engineering, Shenzhen University, Shenzhen 518060, China*

Complete contact information is available at: https://pubs.acs.org/10.1021/acsami.2c10551

Notes

The authors declare no competing financial interest.

ACKNOWLEDGMENTS

This work was supported in part by the Science and Technology Innovation Council of Shenzhen (grant nos. JCYJ20200109105212568, KQTD20170810105439418, 20200812203318002, and 20200810103814002), the National Natural Science Foundation of China (grant no. 61904111), and the Natural Science Foundation of Guangdong Province (grant nos. 2019A1515010790 and 2020A1515011487). The authors thank Mr. Yu Zhang at the Instrumental Analysis Center of Shenzhen University for assistance with the TEM analyses and gratefully acknowledge the Materials and Devices Testing Center of the Graduate School at Shenzhen, Tsinghua University in Shenzhen.

REFERENCES

(1) Anasori, B.; Lukatskaya, M. R.; Gogotsi, Y. 2D Metal Carbides and Nitrides (MXenes) for Energy Storage. *Nat. Rev. Mater.* **2017**, *2*, No. 16098.

(2) Rasool, K.; Pandey, R. P.; Rasheed, P. A.; Buczek, S.; Gogotsi, Y.; Mahmoud, K. A. Water Treatment and Environmental Remediation Applications of Two-Dimensional Metal Carbides (MXenes). *Mater. Today* **2019**, *30*, 80−102.

(3) Huang, K.; Li, Z.; Lin, J.; Han, G.; Huang, P. Two-Dimensional Transition Metal Carbides and Nitrides (MXenes) for Biomedical Applications. *Chem. Soc. Rev.* **2018**, *47*, 5109−5124.

(4) Guo, Z.; Chen, S.; Wang, Z.; Yang, Z.; Liu, F.; Xu, Y.; Wang, J.; Yi, Y.; Zhang, H.; Liao, L.; Chu, P. K.; Yu, X. F. Metal-Ion-Modified Black Phosphorus with Enhanced Stability and Transistor Performance. *Adv. Mater.* **2017**, *29*, No. 1703811.

(5) Xie, Z.; Xing, C.; Huang, W.; Fan, T.; Li, Z.; Zhao, J.; Xiang, Y.; Guo, Z.; Li, J.; Yang, Z.; Dong, B.; Qu, J.; Fan, D.; Zhang, H. Ultrathin 2D Nonlayered Tellurium Nanosheets: Facile Liquid-Phase Exfoliation, Characterization, and Photoresponse with High Performance and Enhanced Stability. *Adv. Funct. Mater.* **2018**, *28*, No. 1705833.

(6) Chhowalla, M.; Liu, Z.; Zhang, H. Two-Dimensional Transition Metal Dichalcogenide (TMD) Nanosheets. *Chem. Soc. Rev.* **2015**, *44*, 2584−2586.

(7) Zhao, M.-Q.; Xie, X.; Ren, C. E.; Makaryan, T.; Anasori, B.; Wang, G.; Gogotsi, Y. Hollow MXene Spheres and 3D Macroporous MXene Frameworks for Na-Ion Storage. *Adv. Mater.* **2017**, *29*, No. 1702410.

(8) Zhao, Z.; Wang, S.; Wan, F.; Tie, Z.; Niu, Z. Scalable 3D Self-Assembly of MXene Films for Flexible Sandwich and Microsized Supercapacitors. *Adv. Funct. Mater.* **2021**, *31*, No. 2101302.

(9) Ma, Z.; Kang, S.; Ma, J.; Shao, L.; Zhang, Y.; Liu, C.; Wei, A.; Xiang, X.; Wei, L.; Gu, J. Ultraflexible and Mechanically Strong Double-Layered Aramid Nanofiber−$Ti_3C_2T_x$ MXene/Silver Nanowire Nanocomposite Papers for High-Performance Electromagnetic Interference Shielding. *ACS Nano* **2020**, *14*, 8368−8382.

(10) Zhu, Y.; Liu, J.; Guo, T.; Wang, J. J.; Tang, X.; Nicolosi, V. Multifunctional $Ti_3C_2T_x$ MXene Composite Hydrogels with Strain Sensitivity toward Absorption-Dominated Electromagnetic-Interference Shielding. *ACS Nano* **2021**, *15*, 1465−1474.

(11) Zeng, Z.; Mavrona, E.; Sacré, D.; Kummer, N.; Cao, J.; Müller, L. A. E.; Hack, E.; Zolliker, P.; Nyström, G. Terahertz Birefringent Biomimetic Aerogels Based on Cellulose Nanofibers and Conductive Nanomaterials. *ACS Nano* **2021**, *15*, 7451−7462.

(12) Wang, L.; Zhang, M.; Yang, B.; Tan, J.; Ding, X. Highly Compressible, Thermally Stable, Light-Weight, and Robust Aramid Nanofibers/Ti_3AlC_2 MXene Composite Aerogel for Sensitive Pressure Sensor. *ACS Nano* **2020**, *14*, 10633−10647.

(13) Ma, Y.; Yue, Y.; Zhang, H.; Cheng, F.; Zhao, W.; Rao, J.; Luo, S.; Wang, J.; Jiang, X.; Liu, Z.; Liu, N.; Gao, Y. 3D Synergistical MXene/Reduced Graphene Oxide Aerogel for a Piezoresistive Sensor. *ACS Nano* **2018**, *12*, 3209−3216.

(14) Zhao, S.; Zhang, H.-B.; Luo, J. Q.; Wang, Q. W.; Xu, B.; Hong, S.; Yu, Z.-Z. Highly Electrically Conductive Three-Dimensional $Ti_3C_2T_x$ MXene/Reduced Graphene Oxide Hybrid Aerogels with Excellent Electromagnetic Interference Shielding Performances. *ACS Nano* **2018**, *12*, 11193−11202.

(15) Zhang, J.; Uzun, S.; Seyedin, S.; Lynch, P. A.; Akuzum, B.; Wang, Z.; Qin, S.; Alhabeb, M.; Shuck, C. E.; Lei, W.; Kumbur, E. C.; Yang, W.; Wang, X.; Dion, G.; Razal, J. M.; Gogotsi, Y. Additive-Free MXene Liquid Crystals and Fibers. *ACS Cent. Sci.* **2020**, *6*, 254−265.

(16) Fan, F. R.; Tian, Z. Q.; Lin Wang, Z. Flexible Triboelectric Generator. *Nano Energy* **2012**, *1*, 328−334.

(17) Zi, Y.; Niu, S.; Wang, J.; Wen, Z.; Tang, W.; Wang, Z. L. Standards and Figure-of-Merits for Quantifying the Performance of Triboelectric Nanogenerators. *Nat. Commun.* **2015**, *6*, No. 8376.

(18) Wu, C.; Wang, A. C.; Ding, W.; Guo, H.; Wang, Z. L. Triboelectric Nanogenerator: A Foundation of the Energy for the New Era. *Adv. Energy Mater.* **2019**, *9*, No. 1802906.

(19) Cheng, L.; Xu, Q.; Zheng, Y.; Jia, X.; Qin, Y. A Self-Improving Triboelectric Nanogenerator with Improved Charge Density and Increased Charge Accumulation Speed. *Nat. Commun.* **2018**, *9*, No. 3773.
(20) Hinchet, R.; Yoon, H.; Ryu, H.; Kim, M.; Choi, E.; Kim, D.; Kim, S. Transcutaneous Ultrasound Energy Harvesting Using Capacitive Triboelectric Technology. *Science* **2019**, *365*, 491−494.
(21) Nie, J.; Wang, Z.; Ren, Z.; Li, S.; Chen, X.; Wang, Z. Power Generation From the Interaction of A Liquid Droplet and A Liquid Membrane. *Nat. Commun.* **2019**, *10*, No. 2264.
(22) Wang, H.; Xu, L.; Bai, Y.; Wang, Z. Pumping Up the Charge Density of a Triboelectric Nanogenerator by Charge-Shuttling. *Nat. Commun.* **2020**, *11*, No. 4203.
(23) Yang, H.; Pang, Y.; Bu, T.; Liu, W.; Luo, J.; Jiang, D.; Zhang, C.; Wang, Z. Triboelectric Micromotors Actuated by Ultralow Frequency Mechanical Mtimuli. *Nat. Commun.* **2019**, *10*, No. 2309.
(24) Zheng, Q.; Tang, Q.; Wang, Z. L.; Li, Z. Self-Powered Cardiovascular Electronic Devices and Systems. *Nat. Rev. Cardiol.* **2021**, *18*, 7−21.
(25) Li, Z.; Chen, J.; Guo, H.; Fan, X.; Wen, Z.; Yeh, M.; Yu, C.; Cao, X.; Wang, Z. Triboelectrification-Enabled Self-Powered Detection and Removal of Heavy Metal Ions in Wastewater. *Adv. Mater.* **2016**, *28*, 2983−2991.
(26) Guo, H.; Pu, X.; Chen, J.; Meng, Y.; Yeh, M.; Liu, G.; Tang, Q.; Chen, B.; Liu, D.; Qi, S.; Wu, C.; Hu, C.; Wang, J.; Wang, Z. A Highly Sensitive, Self-Powered Triboelectric Auditory Sensor for Social Robotics and Hearing Aids. *Sci. Robot.* **2018**, *3*, No. eaat2516.
(27) Li, C.; Liu, D.; Xu, C.; Wang, Z.; Shu, S.; Sun, Z.; Tang, W.; Wang, Z. Sensing of Joint and Spinal Bending or Stretching via A Retractable and Wearable Badge Reel. *Nat. Commun.* **2021**, *12*, No. 2950.
(28) Wang, Y.; Wu, H.; Xu, L.; Zhang, H.; Zhang, H.; Yang, Y.; Yang, Y.; Wang, Z. L. Hierarchically Patterned Self-Powered Sensors for Multifunctional Tactile Sensing. *Sci. Adv.* **2020**, *6*, No. abb9083.
(29) Jin, T.; Sun, Z.; Li, L.; Zhang, Q.; Zhu, M.; Zhang, Z.; Yuan, G.; Chen, T.; Tian, Y.; Hou, X.; Lee, C. Triboelectric Nanogenerator Sensors for Soft Robotics Aiming at Digital Twin Applications. *Nat. Commun.* **2020**, *11*, No. 5381.
(30) Li, N.; Yin, Z.; Zhang, W.; Xing, C.; Peng, T.; Meng, B.; Yang, J.; Peng, Z. A triboelectric-inductive hybrid tactile sensor for highly accurate object recognition. *Nano Energy* **2022**, *96*, No. 107063.
(31) Salauddin, M.; Rana, S. S.; Sharifuzzaman, M.; Rahman, M. T.; Park, C.; Cho, H.; Maharjan, P.; Bhatta, T.; Park, J. Y. A Novel MXene/Ecoflex Nanocomposite-Coated Fabric as a Highly Negative and Stable Friction Layer for High-Output Triboelectric Nanogenerators. *Adv. Energy Mater.* **2020**, *11*, No. 2002832.
(32) Salauddin, M.; Rana, S.; Rahman, M.; Sharifuzzaman, M.; Maharjan, P.; Bhatta, T.; Cho, H.; Lee, S.; Park, C.; Shrestha, K.; Sharma, S.; Park, J. Fabric-Assisted MXene/Silicone Nanocomposite-Based Triboelectric Nanogenerators for Self-Powered Sensors and Wearable Electronics. *Adv. Funct. Mater.* **2022**, *32*, No. 2107143.
(33) Luo, X.; Liu, L.; Wang, Y.; Li, J.; Berbille, A.; Zhu, L.; Wang, Z. Tribovoltaic Nanogenerators Based on MXene-Silicon Heterojunctions for Highly Stable Self-Powered Speed, Displacement, Tension, Oscillation Angle, and Vibration Sensors. *Adv. Funct. Mater.* **2022**, *32*, No. 2113149.
(34) Dong, Y.; Mallineni, S.; Maleski, K.; Behlow, H.; Mochalin, V.; Rao, A.; Gogotsi, Y.; Podila, R. Metallic MXenes: A New Family of Materials for Flexible Triboelectric Nanogenerators. *Nano Energy* **2018**, *44*, 103−110.
(35) Huang, J.; Hao, Y.; Zhao, M.; Li, W.; Huang, F.; Wei, Q. All-Fiber-Structured Triboelectric Nanogenerator via One-Pot Electrospinning for Self-Powered Wearable Sensors. *ACS Appl. Mater. Interfaces* **2021**, *13*, 24774−24784.
(36) Jiang, C.; Wu, C.; Li, X.; Yao, Y.; Lan, L.; Zhao, F.; Ye, Z.; Ying, Y.; Ping, J. All-Electrospun Flexible Triboelectric Nanogenerator Based on Metallic MXene Nanosheets. *Nano Energy* **2019**, *59*, 268−276.
(37) Bhatta, T.; Maharjan, P.; Cho, H.; Park, C.; Yoon, S.; Sharma, S.; Salauddin, M.; Rahman, M.; Rana, S.; Park, J. High-Performance Triboelectric Nanogenerator Based on MXene Functionalized Polyvinylidene Fluoride Composite Nanofibers. *Nano Energy* **2021**, *81*, No. 105670.
(38) Rana, S. M. S.; Rahman, M. T.; Salauddin, M.; Sharma, S.; Maharjan, P.; Bhatta, T.; Cho, H.; Park, C.; Park, J. Y. Electrospun PVDF-TrFE/MXene Nanofiber Mat-Based Triboelectric Nanogenerator for Smart Home Appliances. *ACS Appl. Mater. Interfaces* **2021**, *13*, 4955−4967.
(39) Gao, Y.; Liu, G.; Bu, T.; Liu, Y.; Qi, Y.; Xie, Y.; Xu, S.; Deng, W.; Yang, W.; Zhang, C. MXene Based Mechanically and Electrically Enhanced Film for Triboelectric Nanogenerator. *Nano Res.* **2021**, *14*, 4833−4840.
(40) Jiang, C.; Li, X.; Yao, Y.; Lan, L.; Shao, Y.; Zhao, F.; Ying, Y.; Ping, F. A Multifunctional and Highly Flexible Triboelectric Nanogenerator Based on MXene-enabled Porous Film Integrated with Laser-Induced Graphene Electrode. *Nano Energy* **2019**, *66*, No. 104121.
(41) Cai, Y.-W.; Zhang, X.; Wang, G.; Li, G.; Zhao, D.; Sun, N.; Li, F.; Zhang, H.; Han, J.; Yang, Y. A Flexible Ultra-Sensitive Triboelectric Tactile Sensor of Wrinkled PDMS/MXene Composite Films for E-skin. *Nano Energy* **2021**, *81*, No. 105663.
(42) Cao, W.; Han, O.; Xin, W.; Chao, S.; Ma, C.; Li, Z.; Chen, F.; Ma, M. A Stretchable Highoutput Triboelectric Nanogenerator Improved by MXene Liquid Electrode with High Electronegativity. *Adv. Funct. Mater.* **2020**, *30*, No. 2004181.
(43) Yang, W.; Chen, H.; Wu, M.; Sun, Z.; Gao, M.; Li, W.; Li, C.; Yu, H.; Zhang, C.; Xu, Y.; Wang, J. A Flexible Triboelectric Nanogenerator Based on Cellulose Reinforced MXene Composite Film. *Adv. Mater. Interfaces* **2022**, *9*, No. 2102124.
(44) Feng, Y.; He, M.; Liu, X.; Wang, W.; Yu, A.; Wan, L.; Zhai, J. Alternate-Layered MXene Composite Film-Based Triboelectric Nanogenerator with Enhanced Electrical Performance. *Nanoscale Res. Lett.* **2021**, *16*, No. 81.
(45) Cheng, Y.; Zhu, W.; Lu, X.; Wang, C. Lightweight and Flexible MXene/Carboxymethyl Cellulose Aerogel for Electromagnetic Shielding, Energy Harvest and Self-powered Sensing. *Nano Energy* **2022**, *98*, No. 107229.
(46) Cao, W.-T.; Chen, F.; Zhu, Y.; Zhang, Y.; Jiang, Y.; Ma, M.; Chen, F. Binary Strengthening and Toughening of MXene/Cellulose Nanofiber Composite Paper with Nacre-Inspired Structure and Superior Electromagnetic Interference Shielding Properties. *ACS Nano* **2018**, *12*, 4583−4593.
(47) Zhang, J.; Kong, N.; Uzun, S.; Levitt, A.; Seyedin, S.; Lynch, P.; Qin, S.; Han, M.; Yang, W.; Liu, J.; Wang, X.; Gogotsi, Y.; Razal, J. Scalable Manufacturing of Free-Standing, Strong $Ti_3C_2T_x$ MXene Films with Outstanding Conductivity. *Adv. Mater.* **2020**, *32*, No. 2001093.
(48) Tu, S.; Jiang, Q.; Zhang, X.; Alshareef, H. N. Large Dielectric Constant Enhancement in MXene Percolative Polymer Composites. *ACS Nano* **2018**, *12*, 3369−3377.
(49) Zhao, X.; Xu, H.; Hui, Z.; Sun, Y.; Yu, C.; Xue, J.; Zhou, R.; Wang, L.; Dai, H.; Zhao, Y.; Yang, J.; Zhou, J.; Chen, Q.; Sun, G.; Huang, W. Electrostatically Assembling 2D Nanosheets of MXene and MOF-Derivatives into 3D Hollow Frameworks for Enhanced Lithium Storage. *Small* **2019**, *15*, No. 1904255.
(50) Quero, F.; Nogi, M.; Lee, K.; Poel, G.; Bismarck, A.; Mantalaris, A.; Yano, H.; Eichhorn, S. Cross-Linked Bacterial Cellulose Networks Using Glyoxalization. *ACS Appl. Mater. Interfaces* **2011**, *3*, 490−499.

https://doi.org/10.1021/acsami.2c10551
ACS Appl. Mater. Interfaces 2022, 14, 36741−36752